

Interfacing Neurons with Nanostructured Electrodes Modulates Synaptic Circuit Features

Ana Domínguez-Bajo, Beatriz Loreto Rodilla, Ivo Calaresu, Ana Arché-Núñez, Ankor González-Mayorga, Denis Scaini, Lucas Pérez, Julio Camarero, Rodolfo Miranda, Elisa López-Dolado, María Teresa González,* Laura Ballerini,* and María Concepción Serrano*

Understanding neural physiopathology requires advances in nanotechnology-based interfaces, engineered to monitor the functional state of mammalian nervous cells. Such interfaces typically contain nanometer-size features for stimulation and recording as in cell-non-invasive extracellular microelectrode arrays. In such devices, it turns crucial to understand specific interactions of neural cells with physicochemical features of electrodes, which could be designed to optimize performance. Herein, versatile flexible nanostructured electrodes covered by arrays of metallic nanowires are fabricated and used to investigate the role of chemical composition and nanopopography on rat brain cells in vitro. By using Au and Ni as exemplary materials, nanostructure and chemical composition are demonstrated to play major roles in the interaction of neural cells with electrodes. Nanostructured devices are interfaced to rat embryonic cortical cells and postnatal hippocampal neurons forming synaptic circuits. It is shown that Au-based electrodes behave similarly to controls. Contrarily, Ni-based nanostructured electrodes increase cell survival, boost neuronal differentiation, and reduce glial cells with respect to flat counterparts. Nonetheless, Au-based electrodes perform superiorly compared to Ni-based ones. Under electrical stimulation, Au-based nanostructured substrates evoke intracellular calcium dynamics compatible with neural networks activation. These studies highlight the opportunity for these electrodes to excite a silent neural network by direct neuronal membranes depolarization.

1. Introduction

For decades, scientists have been interested in understanding the state of mammalian cells from different perspectives (e.g., molecular, mechanical, structural, electrical, and functional), as it highly relates to physiology and pathology. In this scenario, recent advances in nanotechnology tools are broadening the technical possibilities to do so. One particular example is the fabrication of interfaces with nanometer-size features for neural stimulation and recording. At present, neural activity can be monitored locally by using intracellular sharp/patch electrodes, extracellular substrate-integrated microelectrode arrays, and fluorescent indicators/genetically encoded probes.^[1] Although advances at the level of individual cells have provided unprecedented knowledge on neuronal functioning, unraveling the connectivity routes of nervous system nuclei and circuits must rely more on the use of cell-non-invasive extracellular microelectrode arrays.^[2–4] By means of nano- and micro-technologies,

A. Domínguez-Bajo, Dr. M. C. Serrano
 Instituto de Ciencia de Materiales de Madrid (ICMM)
 CSIC
 Calle Sor Juana Inés de la Cruz 3
 Madrid 28049, Spain
 E-mail: mc.terradas@csic.es

B. L. Rodilla, A. Arché-Núñez, Dr. L. Pérez, Prof. J. Camarero,
 Prof. R. Miranda, Dr. M. T. González
 Fundación IMDEA Nanociencia
 Calle Faraday 9
 Madrid 28049, Spain
 E-mail: teresa.gonzalez@imdea.org



The ORCID identification number(s) for the author(s) of this article can be found under <https://doi.org/10.1002/adbi.202000117>.

© 2020 The Authors. Published by Wiley-VCH GmbH. This is an open access article under the terms of the Creative Commons Attribution-NonCommercial License, which permits use, distribution and reproduction in any medium, provided the original work is properly cited and is not used for commercial purposes.

DOI: 10.1002/adbi.202000117

B. L. Rodilla, Dr. L. Pérez
 Departamento de Física de Materiales
 Universidad Complutense de Madrid
 Plaza de las Ciencias s/n
 Madrid 28040, Spain

I. Calaresu, Dr. D. Scaini, Prof. L. Ballerini
 International School for Advanced Studies (SISSA/ISAS)
 Via Bonomea 265
 Trieste 34136, Italy
 E-mail: laura.ballerini@sissa.it

A. González-Mayorga, Dr. E. López-Dolado
 Hospital Nacional de Paraplégicos
 SESCAM
 Finca La Peraleda s/n
 Toledo 45071, Spain

Prof. J. Camarero, Prof. R. Miranda
 Instituto “Nicolas Cabrera” and Condensed Matter Physics Center (IFIMAC)
 Departamento de Física de la Materia Condensada
 Universidad Autónoma de Madrid (UAM)
 Campus de Cantoblanco
 Madrid 28049, Spain

the benefits of substrate-integrated extracellular electrode arrays are being combined with those of intracellular electrodes to improve the quality and performance of neural interfaces.^[1,5] Importantly, nanotechnology allows for an improved design of lower impedance and a more intimate interface with individual neurons by better mimicking the native extracellular environment.^[6] Early studies reported the ability of high-density silicon nanowire (NW) transistor arrays to record signals from up to 50 different spatial points in a single axon.^[7] Recent advances in the field include gold mushroom-shaped microelectrodes functionalized with RGD peptides,^[8] vertical NW electrode arrays,^[9] and platinum-black electrodes with nanoscale roughness,^[10] to name a few. Specifically, vertical nanoscale structures have demonstrated to support the growth of a variety of mammalian cells in vitro.^[11] From the chemical point of view, nanoelectrode fabrication has explored materials such as gold (Au),^[12,13] platinum,^[14] silicon,^[9] iridium oxide,^[15] and gallium phosphide.^[16] In these approaches, the reduction in electrode size to the nanometer scale enhances the precision of the stimulation point and then optimizes the efficiency of the stimulating devices.^[17]

Aiming to biomedical applications, the flexibility of the electrodes becomes an essential factor to minimize the mechanical mismatch at the interface and guarantee an effective coupling.^[5] In this line, a series of flexible electrodes have been proposed,^[18–20] but only a few combine flexibility with nanostructure.^[21,22,23] For instance, Rogers and colleagues described a bio-interfaced system based on ultrathin electronics supported by bioresorbable substrates of silk fibroin,^[18] which assures minimal stresses on the tissue and highly conformal coverage. Authors proved the utility of these interfaces to record neural activity in the feline visual cortex. By using a transparent silicone substrate, Mineev et al. patterned microfluidic channels for drug delivery and soft platinum/silicone electrodes and stretchable gold interconnects for electrical stimulation and transferring electrophysiological signals.^[21] This e-dura proved utility for brain-machine interfaces and electrochemical spinal neuromodulation. Differently, vertically aligned carbon nanotubes (CNTs) have been integrated on a flexible and biocompatible parylene substrate to serve as flexible nanostructured electrodes with lower impedance and larger interfacial capacitance for extracellular neuronal recording and stimulation in rats.^[22] On the basis of hydrothermally grown ZnO NWs over a metalized polyimide layer, Ryu et al. described stable flexible neural probes with low impedance after a two steps coating process with gold and PEDOT.^[23] So, in order to achieve flexibility, either non-metallic solutions are used, at the cost of an increase in impedance, or a many-step growth process is required to finally metalize the sample.

In this context, it turns crucial as well to understand the specific interaction of neural cells with topographical features so electrodes can be designed and manipulated to achieve optimized performance and biological responses. Indeed, cells have the ability to respond to topography,^[24] especially in the fate of

progenitor and stem cells.^[25,26] In this sense, Carlberg et al. first demonstrated that topographical cues could be used to induce dopaminergic differentiation of human embryonic stem cells (ESCs) by means of an electrospun polyurethane nanofiber scaffold in the presence of neurotrophic factors.^[27] Other works that followed supported this finding,^[28,29] with polymeric grooved substrates being one of the first and most extensively explored.^[30] Regarding the use of metallic substrates, Au films varying in surface nano-roughness have been proved to induce differential responses in ESCs,^[31] with higher adhesion and differentiation profiles on those films with root mean square surface roughness of ≈ 21 nm rather than 30 nm and plane (0.40 nm). In general terms, surface nanotopography has been stated to significantly accelerate neuronal development in vitro and induce a preferential differentiation of stem cells to neuronal lineages, along with a remarkable impact on neuronal guidance, neurite outgrowth and alignment.^[32,33] In this scenario, pillar structures and NWs are being pursued as a source of “interrupted” topographical features for neural cells, with a wide range of customizable configurations including isotropic and anisotropic forms.^[34] Thus, topographical cues in the shape of pillar structures at the nanoscale are desirable advances to improve spatial control in neural interfacing and to guide relevant biological behaviors.

In this work, we have designed thin metal electrodes whose surface is nanostructured by arrays of vertical metallic NWs grown by template-assisted electrodeposition to improve performance by reducing impedance and more intimately interfacing individual neurons. Differently from most previously reported nanostructured metallic electrodes, the ones presented herein are flexible, allowing an easier implementation in medical interfaces by improving conformal implantation and reducing mechanical stresses on the neural tissue. On the other hand, our technique allows to produce metallic nanostructures in a simple way, guaranteeing a good electrode conductance and low impedance without the need of a multiple-layer growth process. We have investigated the role that both chemical composition and nanotopography play on the biological behavior of rat brain cells in vitro. Morphology, viability and neural differentiation parameters are first studied. We then extend this investigation by challenging the nanostructured electrodes with postnatal hippocampal cultures. Neuronal and glial cells are seeded at the interface of NW arrays to investigate, by confocal microscopy and live calcium imaging, the formation and function of postnatal synaptic networks together with glial cell reactivity. Finally, we verify the ability of these flexible arrays to evoke neuronal action potentials by delivering electrical stimulation and monitoring single cell responses by live calcium imaging.

2. Results and Discussion

2.1. Nanostructured Metallic Arrays Fabrication and Characterization

We fabricated flexible nanostructured electrodes composed of vertical arrays of either gold (Au-NWs) or nickel (Ni-NWs) NWs grown on top of Au substrates. These two different metals were selected to form two different kinds of nanostructured electrodes based on their largely different physicochemical properties.

Dr. E. López-Dolado
Research Unit of “Design and development of biomaterials
for neural regeneration”
Hospital Nacional de Paraplégicos
Joint Research Unit with CSIC
Toledo 45071, Spain

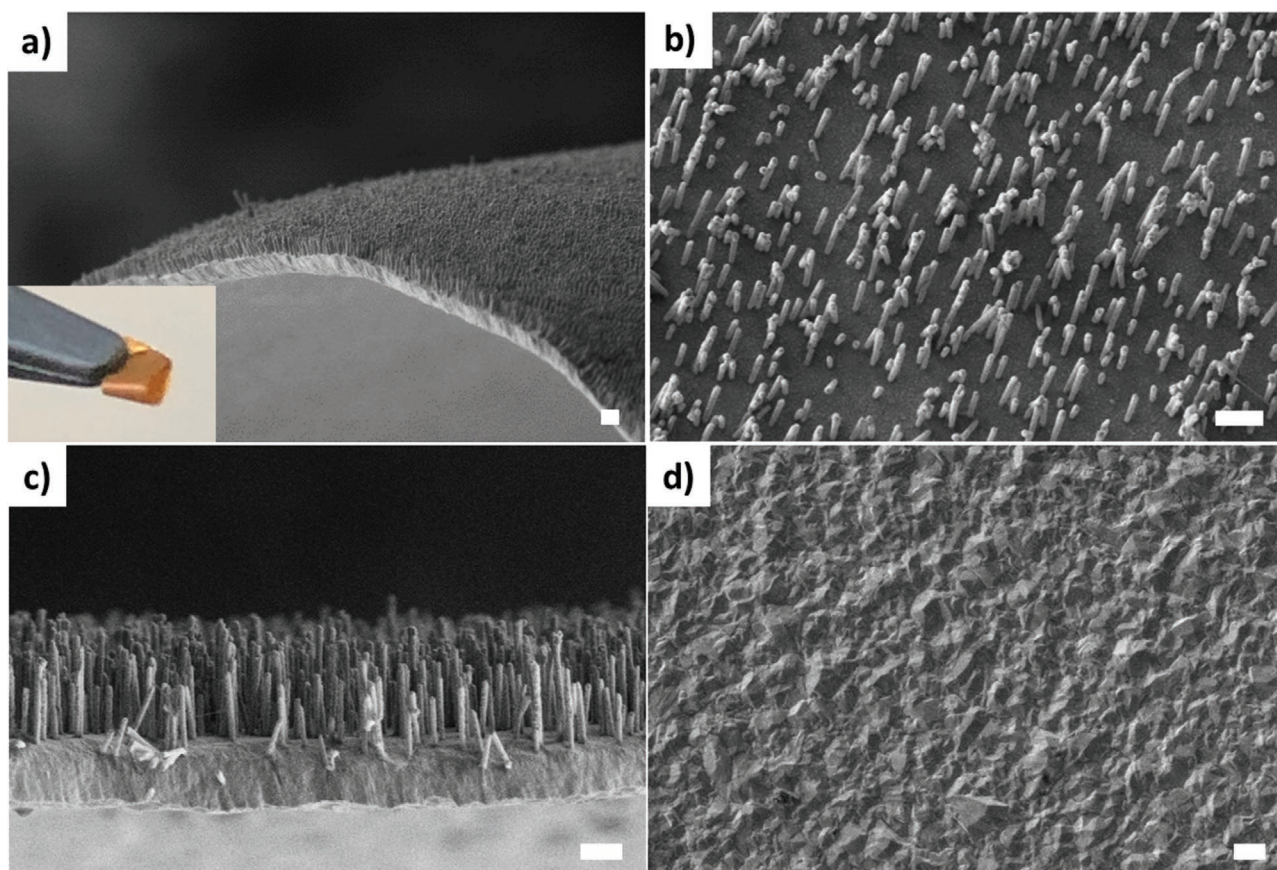


Figure 1. a) Representative SEM image showing the flexibility of the electrodes. SEM image in b) top view and c) cross-section of an Au-NWs electrode in which both, the base and the nanostructured active part can be seen. d) Representative SEM image of a planar Au-Flat electrode. Scale bars represent 1 μm in all the images.

Specifically, the selection of Au was driven by its extensive applicability and biocompatibility, while Ni was chosen by its superior robustness and better mechanical properties than Au. We determined the optimum thickness of the Au substrate to be 1 μm . This is the minimum thickness that preserves both the substrate and the NW-network integrity, allowing the electrode manipulation without damages, while maximizing their flexibility. As illustrated in **Figure 1**, we observed no damage, plastic deformation, break or crack after bending our electrodes with a curvature radius down to 0.3 mm. Importantly, this makes the electrodes adaptable and, therefore, versatile as part of applied neural interfaces.

These arrays were fabricated by template-assisted electro-deposition using polycarbonate nanoporous membranes as templates (details described in the Experimental Section and Figure S1, Supporting Information). After the growth, the template was chemically dissolved, leaving a network of vertical NWs attached at their bottom to the Au flat base. By this methodology, homogeneous and reproducible nanostructured electrodes composed of either Au or Ni NWs were fabricated. Figure 1 shows a representative scanning electron microscopy (SEM) image in top view (panel b) and cross-section (panel c) of an Au-NWs electrode in which both, the base and the nanostructured active part can be seen. Similar images were obtained for Ni-NWs electrodes (Figure S2, Supporting Information). For proper evaluation of the nanostructure effect, we

also fabricated flat electrodes, either composed of Au (Au-Flat) or Ni (Ni-Flat), as reference samples (Figure 1d). Interestingly, we found the impedance of both Au-NWs and Ni-NWs electrodes to be very similar, 106 ± 3 and 108 ± 3 Ω , respectively, which is less than half of the impedance measured in a planar Au electrode of the same area (232 ± 3 Ω), showing that nanostructure clearly reduced the impedance of the electrode as expected, due to a larger electrode effective area. Also, impedance values a 10% lower were observed when bending the NWs electrodes as described above. A denser NWs network covering more tightly the base surface would reduce further the final electrode impedance. We are presently working on obtaining this type of nanostructure.

2.2. Nanotopography and Chemical Composition affect Embryonic Cortical Cell Differentiation In Vitro

To initially assess mammalian brain progenitor fate in contact with the electrodes fabricated, neural cells derived from progenitor cells isolated from the cerebral cortices of rat embryos (rNCCs) were used. Preliminary studies on bare electrodes, either Au-NWs or Ni-NWs, revealed a poor adhesion of these cells, with high-size spheroid-like clumps (Figure S3, Supporting Information). In order to facilitate rNCCs adhesion, samples

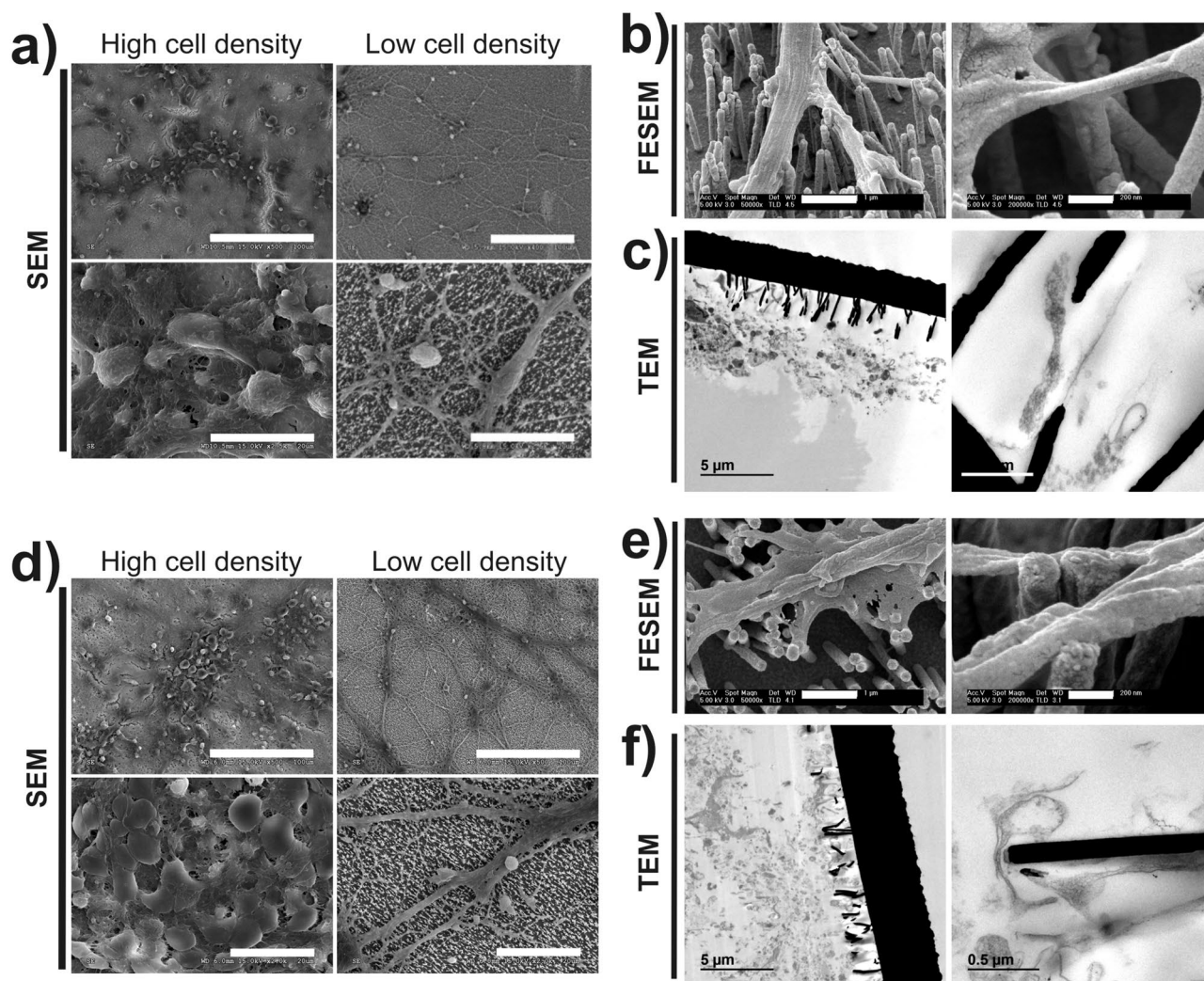


Figure 2. Morphological evaluation of rNCC cultures at high- and low-density seeding conditions on a–c) Au-NWs and d–f) Ni-NWs electrodes. Representative SEM, FESEM, and TEM micrographs of cultures at 14 DIV are shown. Scale bars represent: (a,d) 100 μm (top) and 20 μm (bottom); (b,e): 1 μm (left) and 200 nm (right); and (c,f): 5 μm (left) and 0.5 μm (right).

were thereafter functionalized with poly-L-lysine (PLL) molecules. Immunofluorescence studies with PLL-FITC confirmed the homogeneous functionalization of the arrays surfaces when coated with PLL (Figure S4, Supporting Information). After 14 days in vitro (DIV), rNCCs properly attached and spread on top of PLL-coated Au-NWs platforms colonizing the totality of the substrate surface (Figure 2a) when cultured at favorable high density conditions ($75\,000\text{ cells cm}^{-2}$) as shown by SEM. When challenged at low density ($25\,000\text{ cells cm}^{-2}$), these cells also adhered to the arrays retaining their typical neural morphology and forming interconnected cultures. Detailed observation by field-emission scanning electron microscopy (FESEM) revealed a close contact of both somata and neurites with the Au-NWs (Figure 2b), without evidences of either neural cell membrane piercing or perforation, as also confirmed by transmission electron microscopy (TEM) studies (Figure 2c). Standard glass coverslips served as a reference control material for comparison (Figure S5, Supporting Information). When Ni-NWs electrodes were investigated, a comparable degree of cell adhesion

and close interaction with the NWs arrays surface was found (Figure 2d–f), both at high and low density seeding conditions. Importantly, both Au-NWs and Ni-NWs substrates supported the growth of highly confluent cultures of rNCCs at 21 DIV (Figure S6, Supporting Information). At 28 DIV, however, Ni-NWs electrodes seemed less adhesive to cells than Au-NWs ones so highly compact cell monolayers started to detach (Figure S7, Supporting Information). This inferior performance of Ni substrates with brain cells could be related to some toxicity effects derived from their chemical composition. To this regard, individual Ni NWs produced deleterious effects on diverse cell types such as human WI-38 fibroblasts,^[34] monocytic THP-1 cells^[35] and rat marrow stroma cells.^[36] In HeLa cells, individual Ni NWs (1 μm in length and 50 nm in diameter) induced cell cycle arrest and apoptosis, with significant dose- and length-dependent effects.^[37] We hypothesize that, in our case, the fact of being arranged in a nanostructured array, in which individual wires cannot be internalized by cells, significantly improved cell responses with respect to previous work by others.

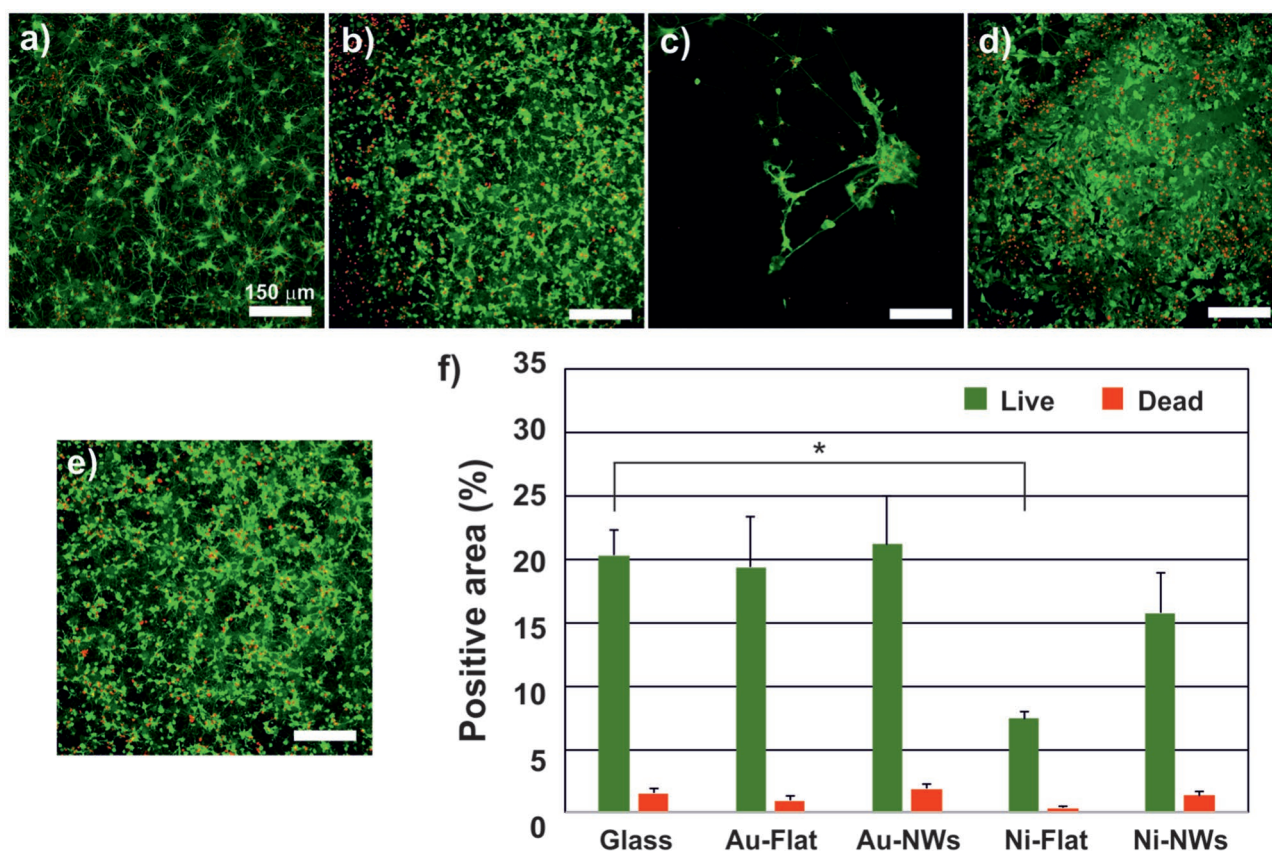


Figure 3. Viability studies of rNCC cultures on the different electrode substrates at 14 DIV by CLSM. Live cells are labeled in green (calcein) and dead cells in red (EthD-1). a) Au-Flat, b) Au-NWs, c) Ni-Flat, d) Ni-NWs electrodes, and e) glass coverslips (control). f) Normalized positive area for alive and dead cells (mean \pm standard deviation; $n \geq 5$ for each condition). Statistics: $*p = 0.021$ (Ni-Flat vs control); one-way ANOVA followed by Games-Howell post-hoc test. For the rest of comparisons, not statistically significant differences were found (one-way ANOVA). Significance symbol: $*p < 0.05$.

In order to elucidate the role that nanotopography might be playing on the neural cell responses found, we next explored equivalent flat electrodes, either fabricated as Au-Flat or Ni-Flat, in comparison to NWs-based ones. rNCC cultures were formed on both flat materials, although cells on Ni-Flat showed a pronounced tendency to clump and fasciculate neurites, as demonstrated by morphological SEM studies (Figure S8, Supporting Information). Then, cell viability was evaluated in all four substrates (Au-Flat, Au-NWs, Ni-Flat, and Ni-NWs) (Figure 3a–e). As these neural cells tend to group in culture and slightly vary in size, it becomes difficult to accurately identify the number of individual live cells, so viability was measured from the images as the area covered by calcein-labelled cells (i.e., live cells). In both types of nanostructured electrodes (Au-NWs and Ni-NWs), a majority of the surface was covered by live cells (green fluorescent as labelled with calcein). When quantified (Figure 3f), cells cultured on nanostructured electrodes were similarly viable to those on control glass substrates (104.3% for Au-NWs and 77.4% for Ni-NWs; $p > 0.999$, Au-NWs vs control, and $p = 0.739$, Ni-NWs vs control). Regarding flat electrodes, while Au-Flat electrodes reached control values, Ni-Flat ones were more poorly colonized than the control with a significantly inferior surface area covered by viable cells ($*p = 0.021$, Ni-Flat vs control), thus demonstrating a significant impact of nanotopography on the survival of rNCCs in the case of Ni-based

electrodes. In agreement with this finding, neural cells in contact with epitaxial gallium phosphide NWs (2.5 μm long and 50 nm wide) also experienced an improvement in cell survival with respect to respective planar substrates.^[38] No statistically significant differences were found when comparing the area of live cells between flat and nanostructured electrodes for each chemical composition (either Au or Ni), although found in the case of Ni-Flat with respect to the control. The area of dead cells was statistically similar in all substrates, including the control, thus indicating an equal degree of cell death sustained in the cultures at 14 DIV.

Differentiation to either neuronal or non-neuronal phenotypes was then investigated by immunofluorescence studies of map-2 (neuronal cytoskeleton protein) and vimentin (non-neuronal cytoskeleton protein) (Figure 4a–e). In both nanostructured electrodes, there was a predominant presence of neuron-differentiated cells, as occurred on control substrates and expected for this cell type and these culture conditions. When quantified (Figure 4f), cells on Au electrodes (both flat and nanostructured) displayed a similar differentiation profile than that found on glass coverslips (map-2: $p = 0.794$, Au-Flat vs control, and $p = 0.248$, Au-NWs vs control; vimentin: $p = 0.380$, Au-Flat vs control, and $p = 0.886$, Au-NWs vs control). On the contrary, on Ni electrodes, rNCC differentiation profiles seemed dependent on both chemical and nanotopography features. While Ni-Flat

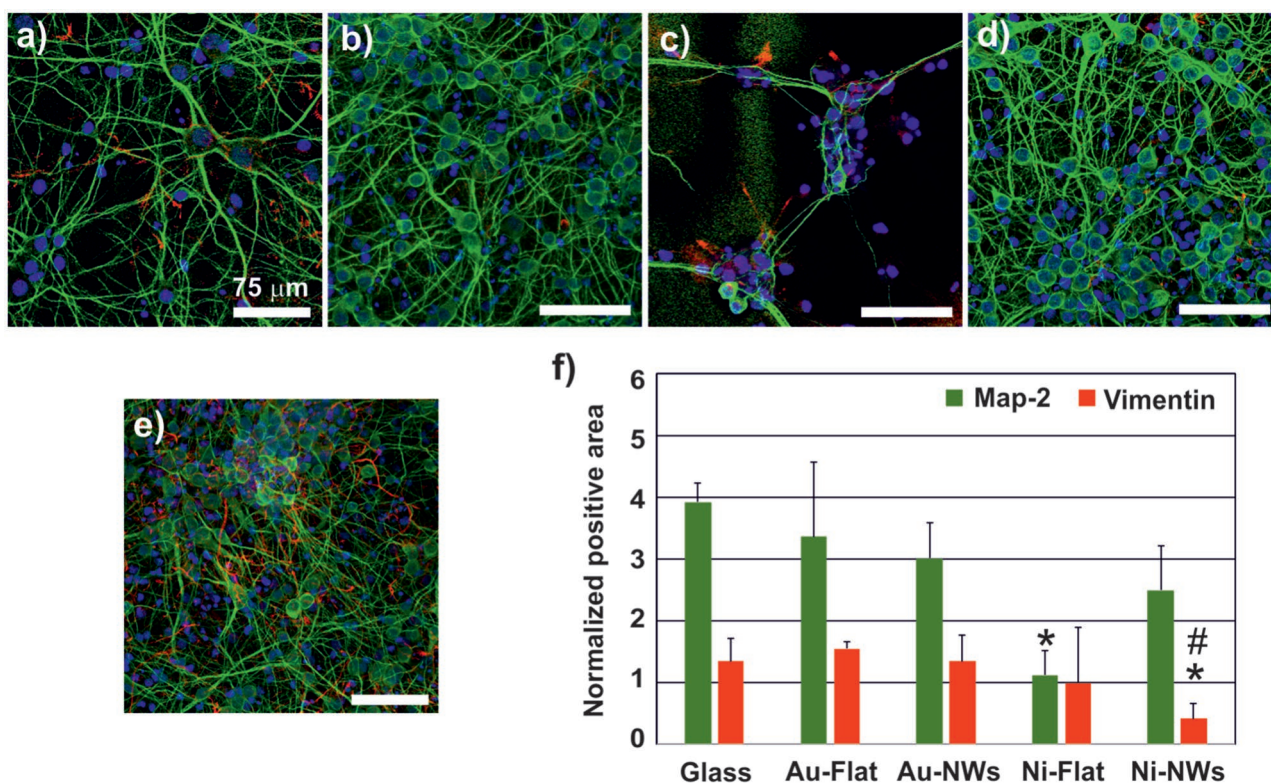


Figure 4. Differentiation studies of rNCC cultures on different electrode substrates at 14 DIV by CLSM. Neurons are labeled for map-2 (green) and non-neuronal cells including glial cells for vimentin (red). In all cases, cell nuclei were stained with DAPI (blue). a) Au-Flat, b) Au-NWs, c) Ni-Flat, d) Ni-NWs electrodes, and e) glass coverslips (control). f) Normalized positive area for neurons (map2⁺) and non-neuronal cells (vimentin⁺) (mean \pm standard deviation; $n \geq 5$ for each condition). Statistics: $*p = 0.037$ (Ni-Flat vs control), $*p = 0.035$ (Ni-NWs vs control) and $\#p = 0.032$ (Ni-NWs vs Au-NWs); in all cases, one-way ANOVA, followed by Games-Howell post-hoc tests. For the rest of comparisons, not statistically significant differences were found (one-way ANOVA). Significance symbol: $*p < 0.05$ in comparisons with respect to control and $\#p < 0.05$ in comparisons to Au-NWs.

substrates hampered neuronal cells appearance ($*p = 0.037$, Ni-Flat vs control), nanostructured ones significantly reduced the presence of glial phenotypes ($*p = 0.035$, Ni-NWs vs control, and $*p = 0.032$, Ni-NWs vs Au-NWs). Based on this, nanotopography features of Ni-based substrates seemed to promote a higher predominance of neurons in comparison to their plane counterparts. This effect, however, was not observed in Au-based electrodes, thus pointing toward an additional role of chemical features on these responses. To this regard, Cho and colleagues described a preferential neuronal differentiation of neural stem cells induced by hierarchically patterned substrates containing both microgroove (1.5 μm) and nanopore (10 nm in diameter) patterns.^[39] At the molecular level, they related these effects to the $\beta 1$ integrin-mediated binding and the intracellular Rho-associated protein kinase pathway. Topography-dependent differentiation patterns have been also described for human ESCs.^[40] Specifically, hESCs preferentially differentiated into neural phenotypes when cultured in anisotropic substrates like gratings, while isotropic patterns including pillars and wells favored their glial differentiation. In this particular approach, topography and size were identified as key parameters to induce cell lineage differentiation. The significant differences in terms of cell type and material configuration (composition, size and inter-distance) of pillars (1 μm in length, 6.5 μm of pitch, and 1 μm in height) with respect to NWs in our study make difficult a direct comparison

and expected the differing biological impact. Interestingly, studies by Stevens and colleagues pointed out toward a synergistic action of nanoscale chemistry and topography on ESCs differentiation when cultured on metallic thin films.^[41]

2.3. Au-NWs Impact Glial Cell Density and Synaptic Activity in Postnatal Hippocampal Cell Cultures

Previous experiments on neural progenitor cells suggested Au-based NWs as the most advantageous material for neural interfacing; so we next challenged such substrates by postnatal hippocampal network. Hippocampal dissociated cultures obtained from rat pups have been extensively used as a standard model for functional studies of nanomaterial-to-neuron interfaces.^[42–46] The morphological adaptation of the most represented cell types in this culture model, namely mature neurons and astrocytes, was therefore investigated. **Figure 5a** shows the appearance of cultured neurons on Au-NWs and compared with Au-Flat and control (glass) substrates, visualized by β -tubulin III immunofluorescence (in red). In all cases, we observed an extensive regrowth of neurites and axons (Figure 5a, left column) and neuronal cell densities were comparable in the three conditions, summarized in the box plot of Figure 5b. When investigating astrocytes by GFAP immunolabelling

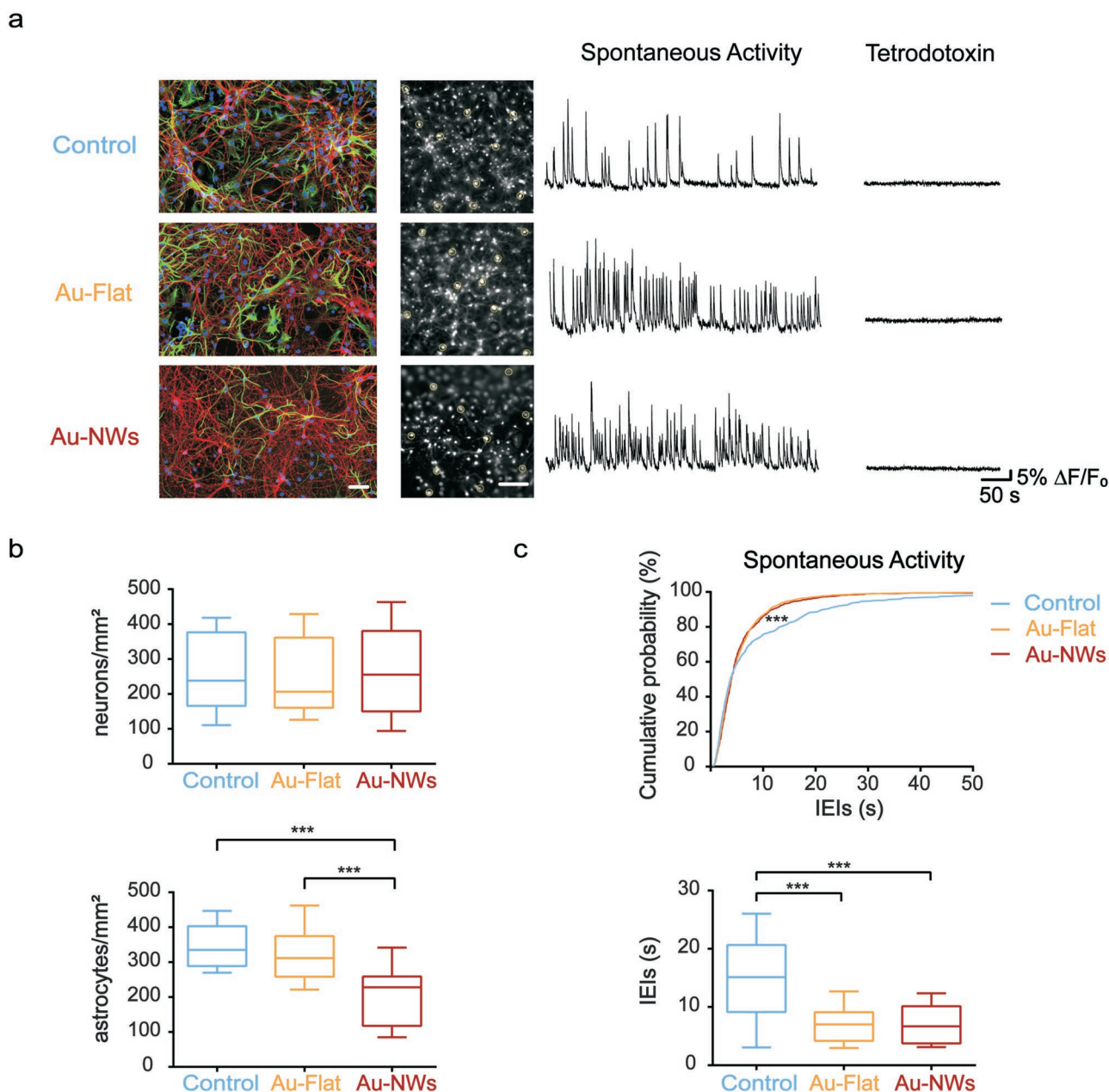


Figure 5. Hippocampal synaptic network formation onto Au-NWs electrodes studied by immunocytochemistry and calcium imaging experiments. a) From left to right, confocal micrographs of immunolabeled cultures, large fields are shown in the first column. Neurons are visualized by anti β -tubulin III, in red, glial cells by anti-GFAP, in green, and nuclei by DAPI, in blue. Scale bar = 100 μ m. Snapshots of 3 representative fields of hippocampal dissociated cultures labeled with Oregon green 488-BAPTA-1 AM. Scale bar = 100 μ m. Yellow circles indicate the selected regions of interest (ROI) from which calcium events were measured. On the right of each field, representative traces of spontaneous network activity for each condition are also shown. TTX was used at the end of each recording to assess the neuronal nature of the signals. Calcium transients are expressed as fractional amplitude increase ($\Delta F/F_0$). b) Left box plots summarize neuronal (top) and astrocytes (bottom) densities in the three conditions ($n = 47$ for control, $n = 39$ for Au-Flat and $n = 44$ for Au-NWs). Statistics: $***p < 0.001$; Kruskal–Wallis test, p -value was adjusted for multiple comparisons with Dunn's correction. c) Top, cumulative probability distribution of the interevent intervals (IEIs); bottom, box plot highlights IEIs distribution around the median values ($n = 42$ for control, $n = 53$ for Au-Flat and $n = 49$ for Au-NWs). Statistics: $***p < 0.001$; both Kolmogorov–Smirnov test and Kruskal–Wallis test on ranks suggested a marked difference in the IEIs distribution among the different substrates, Dunn's correction for multiple comparisons was also used. Significant symbol: $***p < 0.001$ (for both b,c).

(Figure 5a, in green), we detected a significant and selective reduction in GFAP⁺ cell density when cultures were interfaced to the nanostructured surfaces (Au-NWs, 202 ± 96 cells mm^{-2}) in comparison with glass (348 ± 67 cells mm^{-2}) or plane Au

(Au-Flat, 327 ± 88 cells mm^{-2} ; summarized in Figure 5b, lower left box plot, $***p < 0.001$). The lower amount of GFAP⁺ cells in Au-NWs might be relevant for future applications requiring diminished glial reactivity. This seems to be a well-known

feature of nanoscale surface patterning, consisting in a selective reduction of astroglial cell adhesion.^[47] Nonetheless, this was unrelated to Au interaction with cells, since plane Au surfaces showed a comparable astrocyte density to glass. This preferential reduction in glial cells was also found previously with rNCCs cultured on Ni-NWs, not on Au-NWs though, thus evidencing that the specific cell source and inherent characteristics of each neural cell type play a relevant role in the overall biological responses found.

Primary cultured neurons display spontaneous and temporally structured electrical activity.^[45] We explored the network dynamics in hippocampal cultures by calcium imaging, that allows monitoring simultaneously single-cell calcium transients in a population of neurons.^[45] Neurons, stained by a membrane permeable calcium dye, were visualized within the sampled area (Figure 5a, right panels). In all culture groups, we detected spontaneous and repetitive calcium events emerging from episodes of synaptic, action potential-dependent, bursts of activity, fully blocked by tetrodotoxin (TTX) application (Figure 5a, fluorescence tracings). Next, we quantified the occurrence of spontaneous calcium episodes in active cells by measuring the inter-event interval (IEI), the time interval between the onset of a calcium burst and the beginning of the next one. As shown by the cumulative probability distribution and box plots in Figure 5b, Au-Flat and Au-NW substrates increased spontaneous activity, when compared to control, detected as a shift of the IEI toward smaller values ($***p < 0.001$). This peculiar feature was not observed in prior reports where the interaction between plane Au surfaces and hippocampal dissociated cultures was studied at the single-cell level by means of patch-clamp technique.^[46] In this previous study from our group, only PSCs (post-synaptic currents) frequency was monitored via voltage-clamp of single neurons and no indication was provided about the calcium-related collective behavior of the network, which is predominant in our conditions. Indeed, monitoring isolated PSCs provides a measure of synaptic inputs with high temporal resolution, allowing the investigation of individual synaptic changes. Conversely, calcium activity, whose neuronal and synaptic nature was supported by TTX experiments, are reflecting synaptic event due to synchronous firing of neurons, thus reporting neuronal activity occurring at network, more than at cellular resolution.^[45]

2.4. Nanostructured Electrodes Enable Electrical Stimulation of Brain Cell Cultures

Finally, we provide a proof-of-concept for the Au-based substrates to electrically stimulate neural networks in vitro. Regardless the improved network signaling, apparently due to the Au substrates (chemical composition), we further investigated the functionality of Au-based nanoelectrodes in delivering electrical stimulations leading to evoked depolarizations in neurons reaching the threshold for the generation of action potentials. To this aim, we customized a recording chamber to deliver a charge injection from the Au substrates while cultured neurons were monitored by fluorescence calcium imaging (Figure 6a,b, sketch and stimulation protocol). After 10 min of recording of sustained spontaneous synaptic

activity (Figure 6c), a cocktail of synaptic receptor antagonists, containing APV (25×10^{-6} M), BIC (10×10^{-6} M), and CNQX (10×10^{-6} M), was applied to functionally disconnect neurons from the network activity.^[48,49] This condition allowed testing the efficacy of electrical stimuli delivered via the Au substrates in directly depolarizing the monitored neurons, eventually inducing a burst of action potentials. Figure 6d shows such recordings where five biphasic low-voltage steps, repeated three times (Figure 6b, lower left sketch), were delivered either via Au-Flat or Au-NWs electrodes. The observed positive responses are a straightforward link to the ability of Au electrodes to directly depolarize neuronal cell membranes, ultimately leading to evoked action potentials, as confirmed by subsequent TTX application removing all the evoked activity (Figure 6d, underneath traces). These results highlight the possibility to excite a silent network through this novel Au-NWs array by direct neuronal membranes depolarization, leading to action potential propagation. In line with this result, a recent work described a device formed by a forest of randomly oriented Au-coated silicon NWs to enable non-invasive extracellular recording of the slow-frequency oscillations generated by differentiated primary astrocytes.^[50] In this case, flat electrodes failed on recording signals from undifferentiated cells. Differing from array-like configurations, single Au NWs, with a similar diameter to ours but longer lengths (100–200 nm in diameter and over 10 μ m in length), have been also proposed as stimulator/detector systems for electrical stimulation and electrochemical analysis of dopamine exocytosis from PC-12 cells.^[51] These individual electrodes, fabricated by using a vapor transport method,^[52] promoted dopamine release attributed to Ca^{2+} channels opening (pulse voltage tuned from 0.3 to -0.3 V).

Besides their intrinsic interest as advanced platforms for neural stimulation and recording, this type of NWs could also be incorporated into scaffolds to recreate 3D environments for optimal cellular interactions. For example, comparable Au NWs arrays fabricated by template-assisted electrodeposition have been described as highly efficient platforms for the capture and electrochemical release of circulating human leukemic lymphoblasts (tumor cells) when functionalized with aptamers.^[53] By using electrochemical deposition on anodic aluminum oxide as a template, the arrays fabricated were able to capture target cells with much higher yield and to release them with little damage through an electrochemical desorption process. Silicon NWs (150 nm in diameter and 2.6 μ m in length) decorated with Au are being also explored as highly efficient near-infrared (NIR) hyperthermia and photothermal agents for cancer treatment.^[54] Other than metallic, free-standing single coaxial silicon NWs have been recently described as useful materials for photoelectrochemical modulation of neuronal activity.^[55] Curiously, these authors demonstrated that the presence of atomic Au diffused on the NW surface during material growth (where Au nanoclusters were used as a catalyst in a chemical vapor deposition process) enhanced the photoelectrochemical process involved in the stimulation of action potentials in primary rat dorsal root ganglion neurons. The versatility of our fabrication system allow us for the configuration of NWs in the shape of flexible millimeter size arrays as well as individual electrodes if needed, so they can be customized for a plethora of biomedical applications.

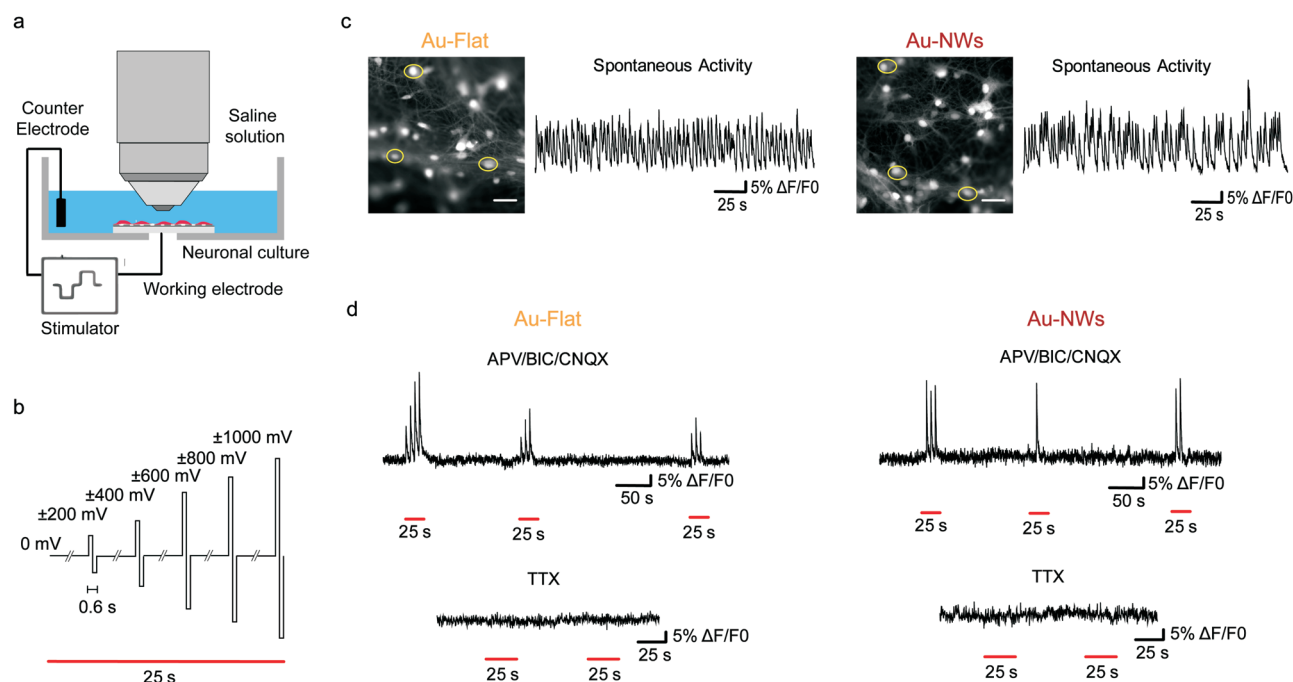


Figure 6. Au-Flat and Au-NWs act as electrode delivering electrical stimulation to cultured neurons. a) A sketch of the experimental setting: a dry connection was ensured between the stimulating electrode and the gold sheets. b) The stimulation protocol applied in this proof-of-concept consisted of five biphasic voltage steps repeated three outdistanced times. Increasing bipolar steps from 0 to 1000 mV were sent at 0.2 Hz and each phase lasted 300 μ s for a total stimulus length of 25 s. c) Two representative snapshot of the imaged field of hippocampal dissociated cultures (scale bar = 50 μ m) grown for 10 DIV onto Au-Flat and Au-NWs electrodes are shown. Cells were labelled with Oregon green 488-BAPTA-1 AM and a circular ROI (region of interest, yellow circle) was drawn around spiking neurons, the mean grey value of the pixels in the ROIs was used to plot the calcium transient course over the time. On the right side of the snapshots a representative trace of the sustained spontaneous synaptic activity corroborates the state of health of tested cells in both conditions. d) The physiological spontaneous synaptic activity of the network was fully blocked (upper traces) by a drug cocktail containing the NMDA receptor antagonist APV (25×10^{-6} M), the GABA_A receptor antagonist BIC (10×10^{-6} M) and the AMPA/kainate receptor antagonist CNQX (10×10^{-6} M). In this condition only stimulus-evoked activity could be observed. Representative fluorescence tracings depict neuronal responses evoked by extracellular pulse stimulations (25 s long red dashes) applied through the Au-Flat (left traces) or Au-NWs electrodes (right traces). Neuronal cells ability to fire action potentials after voltage stimuli was totally abolished by TTX (1×10^{-6} M) treatment (underneath traces) ensuring the neuronal origin of the signals evoked in APV/BIC/CNQX condition. Calcium transients are expressed as fractional amplitude increase in the fluorescence signal ($\Delta F/F_0$, where F_0 is the baseline fluorescence level and ΔF is the rise over baseline).

3. Conclusion

By using Au and Ni as exemplary materials, we have demonstrated that both nanostructure and chemical composition, along with biological features such as cell source and type, play a major role in the interaction of neural cells with electrode arrays. Particularly, Ni-NWs increase neural cell survival, boost neuronal differentiation and reduce glial cell content with respect to their flat counterparts. For Au-based substrates, nanotopography seems to have negligible effects on the survival and differentiation of cortical neural cells. However, Au-NWs induce a significant reduction in glial cell density on primary hippocampal cell cultures when compared to Au-Flat substrates, as also identified on Ni-NWs electrodes. When challenged under electrical stimulation, these Au-NWs substrates sustain intracellular calcium dynamics compatible with functional neural networks. Moreover, our studies highlight the possibility to excite a silent network through these nanostructured arrays by direct neuronal membranes depolarization, leading to action potential propagation.

4. Experimental Section

Material: Chemical reagents and biological molecules were purchased from Sigma-Aldrich and Panreac and used as received, unless otherwise indicated. Antibodies were bought from Sigma-Aldrich and Invitrogen. Neurobasal media and B-27 supplement were purchased from Invitrogen and Thermo Fisher. All additional cell culture media supplements and reagents were obtained from Lonza. All materials and biological samples in this study were manipulated according to standard regulations so no safety concerns arise.

Fabrication and Characterization of Electrodes Covered by Arrays of Metallic NWs: Nanostructured electrodes were prepared by template-assisted electrochemical deposition (schematics shown in Figure S1, Supporting Information) using as templates polycarbonate nanoporous membranes, with 100 nm pore diameter (Whatman). The pores density of the template was 10^8 cm⁻². Electrodeposition was carried out in a three-electrode electrochemical cell with a Metrohm Autolab PGSTAT204 potentiostat, using a Pt mesh as a counter electrode and an Ag/AgCl (3 M NaCl) electrode as a reference electrode. Before electrodeposition, a 100 nm thick Au film was sputtered on one side of the membrane using a Leica EM ACE600 sputtering, which was thickened to 1 μ m using pulse-plating Au electrodeposition, with an on pulse at -1.5 V and an off/rest pulse of 0 V. The use of pulsed electrodeposition allowed to release the stresses during Au thickening, so noncracked flexible Au

thin layers could be obtained. This Au film constituted the base of the final electrode over which the nanowires were deposited. Electrodes with nanowires of either Au (Au-NWs) or Ni (Ni-NWs) were prepared, in order to explore two materials with significantly different physico-chemical properties. For Au electrodeposition, an Orosene commercial electrolyte (ORE+4, Italgalyano) was used at room temperature (RT), with a growth potential of -1.5 V versus RE; whereas for Ni growth a Watts-type electrolyte composed by NiSO_4 (0.8 M), NiCl_2 (0.2 M), and H_3BO_3 (0.4 M), working at 45°C was used, with a growth potential of -1.0 V versus RE. Finally, dichloromethane was used to remove the templates, followed by extensive washing in acetone, ethanol and deionized water, while leaving the network of vertical NWs attached to the Au base. After growth, the morphology of the arrays of metallic NWs was studied by SEM using a ZEISS EVO HD15 microscope. Plane flat Au (Au-Flat) and Ni (Ni-Flat) electrodes were also prepared as reference materials. For Au-Flat, the bases described above were used without performing NW growth, while, for Ni-Flat, a thin Ni layer was deposited on top of the Au bases under the same electrochemical conditions as those used for Ni-NWs growth.

Electrochemical Impedance: The impedance of the electrodes was measured at room temperature by a three-electrode cell using a Metrohm Autolab PGSTAT204 potentiostat with a Pt mesh as a counter electrode and an Ag/AgCl (3 M NaCl) electrode as reference. Measurements were carried out in phosphate buffer saline (PBS) with bovine serum albumin (0.2 mg mL^{-1}), with a modulation of 10 mV at 250 Hz, in circular electrodes of 4 mm in diameter.

Cell Isolation and Culture: Rat Neural Cortical Cells (rNCCs): Neural progenitor cells were obtained from cerebral cortices of E18 Wistar rat embryos as previously described.^[56] All the experimental protocols for cell collection adhered to the regulations of the European Commission (directives 2010/63/EU and 86/609/EEC) and the Spanish government (RD53/2013 and ECC/566/2015) for the protection of animals used for scientific purposes. Adult female Wistar rats were provided by a commercial supplier (Harlan Ibérica, Spain) and sacrificed when gestation reached 16–18 days. A total of 5 independent cell cultures from 5 different animals with a minimum of 3 replicates per condition in each culture were carried out ($N \geq 15$ arrays per condition). The viability of the so-isolated cells was $90 \pm 4\%$ in all cases. For high-density assays, a total of 7.5×10^4 cells contained in a small fraction of media (typically 20 – 50 μL) was seeded on the top part of each array and allowed to attach for 10 min. Immediately after, samples were completely covered with 500 μL of complete Neurobasal media containing: B-27 supplement (2%), streptomycin (100 UI mL^{-1}), penicillin (100 UI mL^{-1}), and L-glutamine (1×10^{-3} M). For low-density assays, cells were seeded at a density of 2.5×10^4 cells cm^{-2} . After 2 h of adhesion in a sterile incubator at 37°C in a CO_2 atmosphere (5%), culture media were replaced and cultures maintained for up to 2 weeks. Culture media were half replaced every 3–4 days. Cell culture was monitored in the periphery of the substrates and control samples by using an Axiovert CFL-40 optical microscope with a coupled Axiocam ICC-1 digital camera (Zeiss). Prior to cell culture, all electrodes were first sterilized by UV radiation in a biosafety cabinet and then functionalized by adsorbing low molecular weight PLL molecules ($30\,000$ – $70\,000$ Da; 45 μg mL^{-1}). The homogeneity of the coating was confirmed by immunofluorescence by using PLL-FITC. Control glass substrates were functionalized following the same protocol as for metallic electrodes.

Cell Isolation and Culture: Rat Hippocampal Cells: Dissociated hippocampal neurons were isolated from post-natal 2–3 days old Wistar rats as previously reported.^[45] Au-Flat and Au-NWs electrodes were washed preliminarily with 5 min long washes on milliQ H_2O and then in ethanol 90% , H_2O and ethanol were previously filtered with 0.22 μm cutoff filter (Merck Millipore). The electrodes were dried at 90°C and their surfaces were activated under low-pressure air plasma (Harrick PDC-32G Plasma Cleaner) for 7 min at RT (20 – 22°C), with RF coil powers of 9 W. A 20 min long exposure to ultraviolet (UV)-radiation was finally used to sterilize the substrates. One hour prior to cell culturing, PLL (50 μg mL^{-1} , Merck) coating was performed onto all tested substrates, including control glass, to enhance positive surface charging,

thus facilitating cell adhesion. About 600 cells mm^{-2} were plated onto control glass, Au-Flat and Au-NWs electrodes, then incubated at 37°C , 5% CO_2 in Neurobasal medium added with B-27 supplement (Thermo Fisher) and GlutaMAX (Thermo Fisher) both to a $1 \times$ final concentration. Gentamicin (5 μg mL^{-1} ; Thermo Fisher) was also added. Cultured cells were grown until 8–12 DIV by renewing half of the medium once in this period.

Cell Morphological Studies by Electron Microscopies: All studied samples were rinsed in PBS twice and fixed with glutaraldehyde (2.5% in PBS) for 45 min as a conventional fixation method for examination by electron microscopy. After washing in distilled water, dehydration was performed by using series of ethanol solutions for 15 min (2 washes) and a final dehydration in absolute ethanol for 30 min. Samples were then dried at RT for at least 24 h. After mounting in stubs and gold coating under vacuum, the morphology of the samples was characterized by using a Hitachi S-3000N electron microscope and a field-emission Philips XL30 S-FEG microscope.

Alternatively, *in vitro* culture samples were first fixed with a mixture of paraformaldehyde 4% and glutaraldehyde 1% in phosphate buffer for 1 h and then post-fixed in osmic tetroxide (1% in distilled water) for an additional hour. Dehydration was then carried out by immersion in successive solutions of ethanol at increasing concentrations (30% , 50% , 70% , 95% , and 100%), with a final step in pure acetone. Samples were included in the resin Durcupán by consecutive immersion steps at increasing concentrations ($1:3$, $1:1$, $3:1$ in acetone). The final samples in pure resin were then polymerized at 60°C for 48 h. Ultrathin sections (≈ 60 nm) were obtained and subsequently stained with uracil acetate and lead citrate. The visualization was carried out by using a Jeol JEM 1010 microscope (Japan) at 80 kV with a coupled camera (Gatan SC200, USA) for image acquisition.

Cell Viability Studies by Confocal Laser Scanning Microscopy (CLSM): To test cell viability, cells cultured on the different substrates were analyzed by using a Live/Dead Viability kit according to manufacturer's instructions. This kit is based on the use of calcein and ethidium homodimer-1 (EthD-1). Calcein is a non-fluorescent cell-permeable dye that gets converted into a strongly green-light emitting compound after contact with intracellular esterases and so retained inside live cells. On the contrary, EthD-1 is a DNA-intercalating agent that penetrates cell membranes in dead cells and emits orange/red fluorescence when inserted into the DNA double helix. After staining, samples were visualized by using a Leica SP5 CLSM. The fluorescence of both probes was excited by an Argon laser tuned to 488 nm. After excitation, emitted fluorescence was separated by using a triple dichroic filter $488/561/633$ and measured at 505 – 570 nm for green fluorescence (calcein) and 630 – 750 nm for red fluorescence (EthD-1). Physical reflection from the metallic electrodes (non-transparent) after excitation at 488 nm was also recorded and used to visualize the material structure and the relative cellular location.

Brain Cells Differentiation Studies by CLSM: rNCC cultures on the different substrates were fixed with paraformaldehyde (4% in PBS) at RT for 12 min and then incubated with the following primary antibodies: 1) Map-2 for somas and dendrites in neurons and 2) Vimentin for non-neuron cells including glial cells. The secondary antibodies used were: Alexa Fluor 488 anti-mouse in goat IgG (H+L) and Alexa Fluor 594 anti-rabbit in goat IgG (H+L) (Life technologies). Both primary and secondary antibodies were dissolved in PBS containing saponin (0.25%) and fetal goat serum (2%) to guarantee cell permeability and to block any non-specific bindings, respectively. Each antibody was incubated for 1 h at RT in darkness. Cell nuclei were labeled with 4',6-diamidino-2-phenylindole (DAPI, 3×10^{-6} M, 5 min). After immunostaining, samples were visualized by using a Leica TCS SP5 microscope. The fluorescence of the different fluorochromes was excited and measured as follows: Alexa Fluor 488 excitation at 488 nm with an argon laser and detection in the range 507 – 576 nm, Alexa Fluor 594 excitation at 594 nm with a helium-neon laser and detection in the range 625 – 689 nm and DAPI excitation at 405 nm with a diode UV laser and detection in the range 423 – 476 nm. Capture conditions in each case were established by using appropriate positive and negative controls and maintained during the

acquisition of all the images. Reflection mode images were taken to observe the metallic electrodes surface in all cases.

Hippocampal cultures were fixed in 4% formaldehyde (prepared from fresh paraformaldehyde) in PBS and permeabilized for 30 min with 0.3% Triton-X-100 (Carlo Erba) in PBS added with 5% FBS (Gibco) and 4% BSA to prevent non-specific binding of primary antibodies. Samples were subsequently incubated with primary antibodies for 30 min at RT and, after being washed with PBS, with secondary antibodies for 45 min. Mounting was performed with anti-fade medium Fluoromount on 1 mm thick microscope glass slides. Neurons were labeled for anti- β -tubulin III and visualized with Alexa 594 anti-rabbit in goat as secondary antibody. Astrocytes were instead stained for GFAP and visualized with Alexa 488 anti-mouse in goat as secondary antibody. Nuclei were stained with DAPI. Nikon Eclipse Ti2 inverted microscope connected to a ATR confocal system was used to acquire confocal reconstructed images ($20 \times$ Plan Apo HL, 0.75 NA).

Calcium Imaging: Hippocampal dissociated cultures were loaded with cell permeable Ca^{2+} dye Oregon Green 488 BAPTA-1 AM (Molecular Probes); $10 \mu\text{L}$ DMSO was added to the stock $50 \mu\text{g}$ of the dye and cultures were incubated with a final concentration of $4 \times 10^{-6} \text{ M}$ for 30 min at 37°C , 5% CO_2 . Samples were therefore placed in a recording chamber mounted on an inverted microscope (Nikon Eclipse Ti-U). Cultures were continuously perfused at 5 mL min^{-1} rate at RT with extracellular saline solution of composition ($\times 10^{-3} \text{ M}$): 150 NaCl, 4 KCl, 2 CaCl_2 , 1 MgCl_2 , 10 HEPES, 10 glucose (pH adjusted to 7.4 with NaOH; osmolarity 300 mOsm). Ca^{2+} -dye was excited at 488 nm with a mercury lamp; excitation light was separated from the light emitted from the sample using a 505 nm dichroic mirror and ND filter (1/32). Oregon loaded cultures were observed with a $20 \times$ objective (PlanFluor, 0.45 NA) and images were continuously acquired (exposure time 150 ms) using an ORCA-Flash4.0 V2 sCMOS camera (Hamamatsu). The imaging system was controlled by an integrating imaging software (HCLImage Live) and the camera was set to operate on 2048×2048 pixels at binning 4. Cultures accustomed to extracellular solution for about 10 min. Spontaneous activity was thereafter recorded for 10 min. At the end of each recording session, $1 \times 10^{-6} \text{ M}$ TTX (a voltage-gated, fast Na^+ channel blocker; Latoxan) was added to confirm the neuronal nature of the recorded signals. 1 field was recorded from each sample and 12 ± 2 cells out of each recording were selected by drawing regions of interest (ROIs) around cell bodies. Images were analyzed with ImageJ software (NIH) and the corresponding traces were studied with Clampfit software (pClamp suite, 10.4 version; Axon Instruments) in off-line mode and with MATLAB (MathWorks, Inc.). The difference between consecutive peaks onset times was computed, to obtain the inter-event interval. Intracellular Ca^{2+} transients were expressed as fractional amplitude increase ($\Delta F/F_0$, where F_0 is the baseline fluorescence level and ΔF is the rise over baseline); the onset time of neuronal activation was determined by detecting those events in the fluorescence signal that exceed at least five times the standard deviation of the noise.^[45]

Spontaneous and Evoked Intracellular Calcium Dynamics Studies under Electrical Stimulation: For the electrical stimulation of the conductive substrates, the bottom of a 35 mm petri dish (Falcon) was modified to include either Au-Flat or Au-NWs squared electrodes of about $6 \times 6 \text{ mm}$. The junction between the petri and the Au-Flat or Au-NWs electrodes was sealed by PDMS silicon elastomer (Sylgard 184 – Down Corning Co.). This setting allowed positioning of a stimulating electrode in direct contact with the Au-Flat and Au-NWs films in a dry environment. In the modified petri dishes, hippocampal cultures were grown for 10 DIV. To deliver stimuli, the positive output of an STG 4002 stimulator (Multi Channel Systems) was plugged to a platinum wire in direct contact with the Au-Flat and Au-NWs electrodes as described above, while the ground output was plugged with an Ag/AgCl pellet electrode submerged in the extracellular saline solution. The extracellular stimulus pattern was designed with MC_Stimulus II (Multi Channel Systems) and the stimulator was controlled by a computer. In these conditions, for calcium live imaging, cells were loaded with the cell permeable Ca^{2+} dye as described above. After incubation, the petri dish with the substrate was mounted in a fixed-stage upright microscope (Eclipse

FN1, Nikon) and was continuously superfused at 5 mL min^{-1} rate, at RT, with the extracellular saline solution (see above). The Ca^{2+} -dye was excited at 488 nm with a mercury lamp; a dichroic mirror and ND filter (1/32) was used to separate the excitation light from the light emitted by the sample. Spontaneous calcium transients were recorded with a $20 \times$ water immersion objective (UMPlanFI, 0.5 NA, Olympus) using an EMCCD camera (IXon Ultra 897, AndorTM, Oxford Instruments) controlled by a computer through NIS-elements D (Nikon). Images were acquired each 150 ms at 10 MHz readout compensating the read noise with $250 \times$ electron multiplying (EM) gain. 20 min of basal spontaneous activity was recorded then the following antagonists were applied: APV $25 \times 10^{-6} \text{ M}$ (glutamate NMDA receptor selective antagonist), bicuculline $10 \times 10^{-6} \text{ M}$ (BIC, GABA_A receptor antagonist) and CNQX $10 \times 10^{-6} \text{ M}$ (glutamate AMPA/kainate receptor antagonist) to remove all ongoing synaptic activity.^[46] This experimental condition was used to detect the evoked Ca^{2+} transients due to direct excitation of cells and generation of action potentials via either Au-Flat or Au-NWs electrodes electrical stimulation. The neuronal nature of the recorded calcium episodes was ensured by applying $1 \times 10^{-6} \text{ M}$ TTX which readily abolished any evoked responses. All off line analyses were accomplished by the ImageJ software (NIH) and the Clampfit software (pClamp suite, 10.4 version; Axon Instruments).

Statistical Analysis: The procedure used for the quantification of the immunofluorescence images from viability and differentiation studies of rNCCs was based on an automatized protocol created by using the Fiji software in which the observer must only define a threshold of positive staining for each marker established from the negative controls. In order to minimize bias effects, quantifications were carried out blind by two independent observers. The positively stained area for each particular marker was expressed as a percentage of the total image area. Quantified parameters were expressed as the mean \pm standard deviation. For each parameter under study and substrate, images were randomly acquired from a minimum of 3 independent experiments ($n \geq 5$). For parametric analysis to compare more than 2 groups, one-way analyses of variance (ANOVA) followed by either Scheffé or Games–Howell post-hoc tests (homogeneous and heterogeneous variances, respectively, according to Levene's test) was used. For non-parametric analysis, the Mann–Whitney U test was used for comparisons between groups. In studies with rNCCs, the statistical significance levels were defined as: $*p < 0.05$, $**p < 0.01$, and $***p < 0.005$. Statistical analyses were performed by using the Statistical Package for the Social Sciences software (SPSS, version 17.0).

Quantitative data for neuronal and astrocytes densities from hippocampal cells were presented as box plots. Images were randomly acquired from 3 independent culture series, 4 cultures each, and at least 3 fields per culture dish. Statistical comparisons were done by the Kruskal–Wallis test, being the p -value adjusted for multiple comparisons with Dunn's correction. Distribution of IELs in hippocampal cells was presented as cumulative probability and box plots. Calcium imaging was recorded in hippocampal cells from at least 3 independent cultures per treatment. Statistical comparisons were done by the Kolmogorov–Smirnov test and the Kruskal–Wallis test on ranks, using also Dunn's correction for multiple comparisons. In studies with hippocampal cells, the statistical significance level was defined as: $***p < 0.001$. Statistical analyses in this case were performed by using the Prism 6 software.

Supporting Information

Supporting Information is available from the Wiley Online Library or from the author.

Acknowledgements

A.D.-B. and B.L.R. contributed equally to this work. This work was funded by the European Union's Horizon 2020 research and innovation

programme under grant agreement No. 737116 (ByAxon). The work was also partially funded by the Spanish Ministry of Science and Innovation through project BiSURE (Grant: DPI2017-90058-R) and the 'Severo Ochoa' Programme for Centers of Excellence in R&D (MINECO, Grant SEV-2016-0686), as well as by the Comunidad de Madrid project NanoMagCOST (CM S2018/NMT-4321). BLR acknowledges UCM for her predoctoral fellowship. Authors are thankful to Dr. Esperanza Salvador, Isidoro Poveda, Gabriel Carro, Enrique Rodríguez, Dr. Francisco Urbano, and Dr. Covadonga Agudo from the Servicio Interdepartamental de Investigación at the Universidad Autónoma de Madrid for respective assistance with SEM, FESEM, and TEM studies. Sylvia Gutiérrez from the Advanced Light Microscopy Service at the Centro Nacional de Biotecnología (CNB-CSIC) is acknowledged for her assistance with CLSM studies.

Conflict of Interest

The authors declare no conflict of interest.

Keywords

electrical stimulation, electrode arrays, metallic nanowires, nanotopography, neural interfaces

Received: May 2, 2020

Revised: July 16, 2020

Published online: August 6, 2020

- [1] M. E. Spira, A. Hai, *Nat. Nanotechnol.* **2013**, *8*, 83.
- [2] M. E. Spira, S. H. Huang, N. Shmoel, H. Erez, *Adv. Neurobiol.* **2019**, *22*, 125.
- [3] D. Eytan, S. Marom, *J. Neurosci.* **2006**, *26*, 8465.
- [4] T. J. Blanche, M. A. Spacek, J. F. Hetke, N. V. Swindale, *J. Neurophysiol.* **2005**, *93*, 2987.
- [5] M. N. Hasan, A. N. Radwan, M. Kim, E. Kucukal, D. Maji, V. Pashaei, C.-Y. Chung, A. Kakkar, U. A. Gurkan, *Technology* **2019**, *07*, 57.
- [6] S. K. Seidlits, J. Y. Lee, C. E. Schmidt, *Nanomedicine* **2008**, *3*, 183.
- [7] F. Patolsky, B. P. Timbo, G. Yu, Y. Fang, A. B. Greytak, G. Zheng, C. M. Lieber, *Science* **2006**, *313*, 1100.
- [8] A. Hai, J. Shappir, M. E. Spira, *J. Neurophysiol.* **2010**, *104*, 559.
- [9] J. T. Robinson, M. Jorgolli, A. K. Shalek, M. H. Yoon, R. S. Gertner, H. Park, *Nat. Nanotechnol.* **2012**, *7*, 180.
- [10] J. Abbott, T. Ye, K. Krenke, R. S. Gertner, S. Ban, Y. Kim, L. Qin, W. Wu, H. Park, D. Ham, *Nat. Biomed. Eng.* **2020**, *4*, 232.
- [11] A. F. McGuire, F. Santoro, B. Cui, *Ann. Rev. Anal. Chem.* **2018**, *11*, 101.
- [12] M. Dipalo, H. Amin, L. Lovato, F. Moia, V. Caprettini, G. C. Messina, F. Tantussi, L. Berdondini, F. De Angels, *Nano Lett.* **2017**, *17*, 3932.
- [13] D. Brüggemann, B. Wolfrum, V. Maybeck, Y. Mourzina, M. Jansen, A. Offenhäusser, *Nanotechnology* **2011**, *22*, 265104.
- [14] C. Xie, Z. Lin, L. Hanson, Y. Cui, B. Cui, *Nat. Nanotechnol.* **2012**, *7*, 185.
- [15] Z. C. Lin, C. Xie, Y. Osakada, Y. Cui, B. Cui, *Nat. Commun.* **2014**, *5*, 3206.
- [16] D. B. Suyatin, L. Wallman, J. Thelin, C. N. Prinz, H. Jörntell, L. Samuelson, L. Montelius, J. Schouenborg, *PLoS ONE* **2013**, *8*, e56673.
- [17] G. M. Dittami, R. D. Rabbitt, *Lab Chip* **2010**, *10*, 30.
- [18] D. H. Kim, J. Viventi, J. J. Amsden, J. Xiao, L. Vigeland, Y. S. Kim, J. A. Blanco, B. Panilaitis, E. S. Frechette, D. Contreras, D. L. Kaplan, F. G. Omenetto, Y. Huang, K. C. Hwang, M. R. Zakin, B. Litt, J. A. Rogers, *Nat. Mater.* **2010**, *9*, 511.
- [19] Z. J. Sperry, K. Na, S. S. Parizi, H. J. Chiel, J. Seymour, E. Yoon, T. M. Bruns, *J. Neural Eng.* **2018**, *15*, 036027.
- [20] S. Huang, Y. Liu, Y. Zhao, Z. Ren, C. F. Guo, *Adv. Funct. Mater.* **2019**, *29*, 1805924.
- [21] I. R. Mineev, P. Musienko, A. Hirsch, Q. Barraud, N. Wenger, E. M. Morand, J. Gandar, M. Capogrosso, T. Milekovic, L. Asboth, R. F. Torres, N. Vachicouras, Q. Liu, N. Pavlova, S. Duis, A. Larmagnac, J. Vörös, S. Micera, Z. Suo, G. Courtine, S. P. Lacour, *Science* **2015**, *347*, 159.
- [22] W. Yi, C. Chen, Z. Feng, Y. Xu, C. Zhou, N. Masurkar, J. Cavanaugh, M. M. Cheng, *Nanotechnology* **2015**, *26*, 125301.
- [23] M. Ryu, J. H. Yang, Y. Ahn, M. Sim, K. H. Lee, K. Kim, T. Lee, S.-J. Yoo, S. Y. Kim, C. Moon, M. Je, J.-W. Choi, Y. Lee, J. E. Jang, *ACS Appl. Mater. Interfaces* **2017**, *9*, 10577.
- [24] D. Jain, S. Mattiassi, E. L. Goh, E. K. F. Yim, *Neural Regen. Res.* **2020**, *15*, 573.
- [25] D. E. Discher, D. J. Mooney, P. W. Zandstra, *Science* **2009**, *324*, 1673.
- [26] D. Hoffman-Kim, J. A. Mitchel, R. V. Bellamkonda, *Annu. Rev. Biomed. Eng.* **2010**, *12*, 203.
- [27] B. Carlberg, M. Z. Axell, U. Nannmark, J. Liu, H. G. Kuhn, *Biomed. Mater.* **2009**, *4*, 045004.
- [28] M. R. Lee, K. W. Kwon, H. Jung, H. N. Kim, K. Y. Suh, K. Kim, K. S. Kim, *Biomaterials* **2010**, *31*, 4360.
- [29] E. Shhbazi, S. Kiani, H. Gourabi, H. Baharvand, *Tissue Eng., Part A* **2011**, *17*, 3021.
- [30] C. H. Chen, C. C. Tsai, P. T. Wu, I. K. Wang, J. Yu, W. B. Tsai, *ACS Appl. Mater. Interfaces* **2019**, *2*, 205.
- [31] G. J. Bakeine, J. Ban, G. Greci, A. Pozzato, S. Dal Zilio, M. Prasciolu, L. Businaro, M. Tormen, M. E. Ruaro, *Microelectron. Eng.* **2009**, *86*, 1435.
- [32] H. K. Kim, E. Kim, H. Jang, Y. K. Kim, K. Kang, *ChemNanoMat* **2017**, *3*, 278.
- [33] M. Marcus, K. Baranes, M. Park, I. S. Choi, K. Kang, O. Shefi, *Adv. Healthc. Mater.* **2017**, *6*, 1700267.
- [34] L. P. Felix, J. E. Perez, M. F. Contreras, T. Ravasi, J. Kosel, *Toxicol. Rep.* **2016**, *3*, 373.
- [35] F. Byrne, A. Prina-Mello, A. Whelan, B. M. Mohamed, A. Davies, Y. K. Gurko, J. M. D. Coey, Y. Volkov, *J. Magn. Magn. Mater.* **2009**, *321*, 1341.
- [36] A. Prina-Mello, Z. Diao, J. M. Coey, *J. Nanobiotechnol.* **2006**, *4*, 9.
- [37] C. G. Ma, M. M. Song, Y. Zhang, M. Q. Yan, M. Zhang, H. Bi, *Toxicol. Rep.* **2014**, *1*, 114.
- [38] W. Hällström, T. Martensson, C. Prinz, P. Gustavsson, L. Montelius, M. Kanje, *Nano Lett.* **2007**, *7*, 2960.
- [39] K. Yang, H. Jung, H. R. Lee, J. S. Lee, S. R. Kim, K. Y. Song, E. Cheong, J. Bang, S. G. Im, S. W. Cho, *ACS Nano* **2014**, *8*, 7809.
- [40] S. Ankam, M. Suryana, L. Y. Chan, A. A. K. Moe, B. K. K. Teo, J. B. K. Law, M. P. Sheetz, H. Y. Low, E. K. F. Yim, *Acta Biomater.* **2013**, *9*, 4535.
- [41] V. L. S. LaPointe, A. T. Fernandes, N. C. Bell, F. Stellacci, M. M. Stevens, *Adv. Healthcare Mater.* **2013**, *2*, 1644.
- [42] G. Cellot, F. M. Toma, Z. K. Varley, J. Laishram, A. Villari, M. Quintana, S. Cipollone, M. Prato, L. Ballerini, *J. Neurosci.* **2011**, *31*, 12945.
- [43] S. Li, F. P. Ulloa Severino, J. Ban, L. Wang, G. Pinato, V. Torre, Y. Chen, *Biomed. Mater.* **2018**, *13*, 034105.
- [44] F. P. Ulloa Severino, J. Ban, Q. Song, M. Tang, G. Bianconi, G. Cheng, V. Torre, *Sci. Rep.* **2016**, *6*, 29640.
- [45] S. Bosi, R. Rauti, J. Laishram, A. Turco, D. Lonardoni, T. Nieuw, M. Prato, D. Scaini, L. Ballerini, *Sci. Rep.* **2015**, *5*, 9562.
- [46] N. P. Pampaloni, M. Lottner, M. Giugliano, A. Matruglio, F. D'Amico, M. Prato, J. A. Garrido, L. Ballerini, D. Scaini, *Nat. Nanotechnol.* **2018**, *13*, 755.
- [47] C. Vallejo-Giraldo, K. Krukiewicz, I. Calaresu, J. Zhu, M. Palma, M. Fernandez-Yague, B. W. McDowell, N. Peixoto, N. Farid,

- G. O'Connor, L. Ballerini, A. Pandit, M. J. P. Biggs, *Small* **2018**, *14*, 1800863.
- [48] I. Rago, R. Rauti, M. Bevilacqua, I. Calaresu, A. Pozzato, M. Cibilin, M. Dalmiglio, C. Tavagnacco, A. Goldoni, D. Scaini, *Adv. Biosyst.* **2019**, *3*, 1800286.
- [49] S. Stern, A. Agudelo-Toro, A. Rotem, E. Moses, A. Neef, *PLoS ONE* **2015**, *10*, e0132577.
- [50] E. Saracino, L. Maiolo, D. Polese, M. Semprini, A. I. Borrachero-Conejo, J. Gasparetto, S. Murtagh, M. Sola, L. Tomasi, F. Valle, L. Pazzini, F. Formaggio, M. Chiappalone, S. Hussain, M. Caprini, M. Muccini, L. Ambrosio, G. Fortunato, R. Zamboni, A. Convertino, V. Benfenati, *Adv. Biosyst.* **2020**, *4*, 1900264.
- [51] M. Kang, S. M. Yoo, R. Gwak, G. Eom, J. Kim, S. Y. Lee, B. Kim, *Nanoscale* **2016**, *8*, 214.
- [52] Y. Yoo, K. Seo, S. Han, K. S. K. Varadwaj, H. Y. Kim, J. H. Ryu, H. M. Lee, J. P. Ahn, H. Ihee, B. Kim, *Nano Lett.* **2010**, *10*, 432.
- [53] T. T. Zhai, D. Ye, Q. W. Zhang, Z. Q. Wu, X. H. Xia, *ACS Appl. Mater. Interfaces* **2017**, *9*, 34706.
- [54] A. Convertino, V. Mussi, L. Maiolo, M. Ledda, M. G. Lolli, F. A. Bovino, G. Fortunato, M. Rocchia, A. Lisi, *Nanotechnology* **2018**, *29*, 415102.
- [55] R. Parameswaran, J. L. Carvalho-de-Souza, Y. Juang, M. J. Burke, J. F. Zimmerman, K. Koehler, A. Philips, J. Yi, E. J. Adams, F. Bezanilla, B. Tian, *Nat. Nanotechnol.* **2018**, *13*, 260.
- [56] M. Carballo-Vila, B. Moreno-Burriel, E. Chinarro, J. R. Jurado, N. Casañ-Pastor, J. E. Collazos-Castro, *J. Biomed. Mater. Res., Part A* **2009**, *90A*, 94.